Supporting Information

A Bio-Inspired Sustainable Sugar Battery Integrated with a Reversible Coordination Complex

Bhojkumar Nayak[a,‡], Abdul Raafik Arattu Thodika[a,‡], Vinay Pandey[a], Mruthyunjayachari Chattanahalli Devendrachari[a], Neethu Christudas Dargily[a], Rohit Srivastava[b,*], Ahmad Umar[c,d,*], Musthafa Ottakam Thotiyl[a,*]

[a]*Department of Chemistry, Indian Institute of Science Education and Research (IISER)-Pune, Dr. Homi Bhabha Road, Pashan, Pune 411008, Maharashtra, India.*

E-mail: musthafa@iiserpune.ac.in

[b]Department of Petroleum Engineering School of Energy Technology, Pandit Deendayal Energy University, Gandhinagar, Gujarat, India, 382007

Email: rohit.s@spt.pdpu.ac.in

[c]*Department of Chemistry, College of Science and Arts, Najran University, Najran-11001, Kingdom of Saudi Arabia*

[d]*Department of Materials Science and Engineering, The Ohio State University, Columbus, Ohio, USA*

Email: ahmadumar786@gmail.com

[‡]*These authors contributed equally*

Experimental Sections

Materials and reagents:

D-glucose ($C_6H_{12}O_6$), Galactose ($C_6H_{12}O_6$), Mannose ($C_6H_{12}O_6$), Sucrose ($C_{12}H_{22}O_{11}$), Potassium ruthenium(II) hexamine chloride ($[Ru(NH_3)_6]^{3+}$), N,N-(dimethylaminomethyl) ferrocene (*N*-ferrocene), potassium ferrocyanide/ferricyanide, ferrocene, and tris(bipyridine) ruthenium(II) chloride ($[Ru(bpy)_3]^{2+}$), hydrogen peroxide (H_2O_2), Nafion solution (5%), Conc. H_2SO_4 (98%), Potassium nitrate (KNO_3), sodium hydroxide (NaOH), isopropyl alcohol (IPA) were obtained from Sigma Aldrich, Alfa Aesar, and Rankem, India. Toray carbon sheets (GDL), Pt/C and Nafion-117 membrane were procured from fuel cell store, USA.

Three electrode electrochemical study:

Cyclic voltammetry, linear sweep voltammetry, and chronopotentiometry were conducted using a Biologic VMP-300 workstation in a standard three-electrode setup. The working electrodes included platinum (Pt), glassy carbon (GC), and gold (Au), with Hg/HgO serving as the reference electrode and Pt as the counter electrode. Before testing, all working electrodes were meticulously polished with 0.05 µm alumina slurry and electrochemically cleaned by potential cycling in the test electrolyte until stable electrochemical responses were achieved. For the Au electrode, cleaning involved cycling through its oxide formation and reduction potentials. Cyclic voltammograms of monosaccharides (glucose, galactose, mannose) and sucrose were recorded on the Pt electrode. The study also investigated various redox systems, including potassium ruthenium(II) hexamine chloride ($[Ru(NH_3)_6]^{3+}$), N,N-(dimethylaminomethyl) ferrocene (N-ferrocene), potassium ferrocyanide/ferricyanide, ferrocene, and tris(bipyridine) ruthenium(II) chloride ($[Ru(bpy)_3]^{2+}$), all in 1 M KNO_3 electrolyte. Additionally, scan rate dependence cyclic voltammetry was performed using glassy carbon as the working electrode.

Hydrodynamic study:

Rotating disk electrode (RDE) experiments were performed using a PARSTAT MC electrochemical workstation (Amatek) to determine the electron transfer number during the ferricyanide reduction. The current responses were measured across rotation rates ranging from 100 to 3600 rpm in an electrolyte containing 10 mM $K_3[Fe(CN)_6]$. The electrochemical kinetics were analyzed using the Levich equation:

$$I_L = 0.62\, n\, F\, A\, D^{2/3}\, v^{-1/6}\, C\, \omega^{1/2}$$

where I_L= Levich current (A), n= number of electrons, F= Faraday constant (C/mol), A= area of the electrode in cm^2, D= diffusion coefficient (cm^2/s), C= concentration (mol/cm^3), v= kinematic viscosity (cm^2/s), ω= angular rotation rate of the electrode (rad/s). Linear regression of the Levich plot (limiting current density vs. √ω)

yielded a slope corresponding to n ≈ 1, confirming the single-electron reduction of $[Fe(CN)_6]^{3-}$ to $[Fe(CN)_6]^{4-}$. This result agrees with the theoretically expected one-electron redox process for the ferricyanide/ferrocyanide redox couple, validating our experimental approach and supporting subsequent electrochemical analyses.

Device level assembly:

The bio-inspired sustainable sugar battery (glucose–ferricyanide system) was assembled in a dual-chamber configuration separated by a pretreated Nafion 117 cation-exchange membrane. Prior to use, the membrane was activated by sequential boiling in an acidic H_2O_2 solution at 80 °C, followed by storage in a NaOH solution. The anode chamber contained 15 mL of 2 M glucose in 1 M NaOH and employed a Pt/C catalyst (0.5 mg/cm^2) coated on 0.3 mm thick Toray carbon paper. The cathode chamber contained 15 mL of 0.5 M potassium ferricyanide in 1 M NaOH, with a 0.3 mm thick Toray carbon paper electrode serving as the driving electrode. Both chambers were purged with nitrogen for 30 minutes prior to measurements to establish anaerobic conditions.

The glucose–air fuel cell was fabricated using a conventional fuel cell configuration. For comparison, the glucose–air fuel cell was fabricated as a membrane electrode assembly by sandwiching a pretreated Nafion 117 membrane between anodic and cathodic Pt/C catalyst layers (0.5 mg/cm^2) coated on 0.3 mm thick Toray carbon paper. The MEA was hot-pressed at 130 °C for 3 minutes prior to electrochemical testing. Performance was obtained at room temperature for both devices.

Characterization techniques:

Various analytical techniques and instruments were employed to characterize the system. Ultraviolet-visible (UV-vis) spectroscopy was performed using a PerkinElmer Lambda 950 instrument. FT-IR spectra were recorded using the Bruker Platinum ATR spectrometer system, and Nuclear Magnetic Resonance (NMR) spectra were obtained using a Bruker 400 MHz spectrometer. In situ UV–vis spectroelectrochemistry was performed to identify the species during oxidation and reduction using an ALS SEC2000 UV–vis spectrometer.

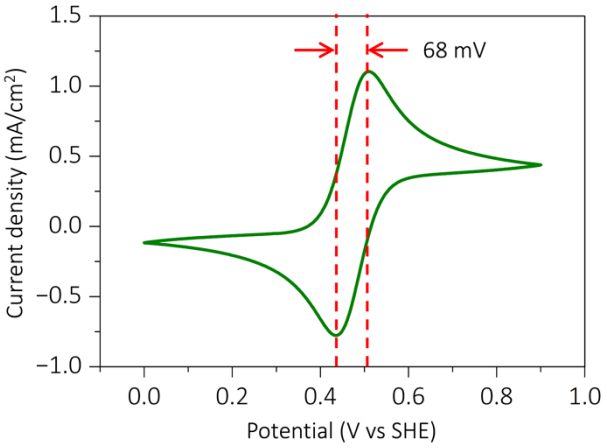

Fig. S1: Cyclic voltammograms of 10 mM ferrocyanide in 1 M KNO_3 at 20 mV/s scan rate.

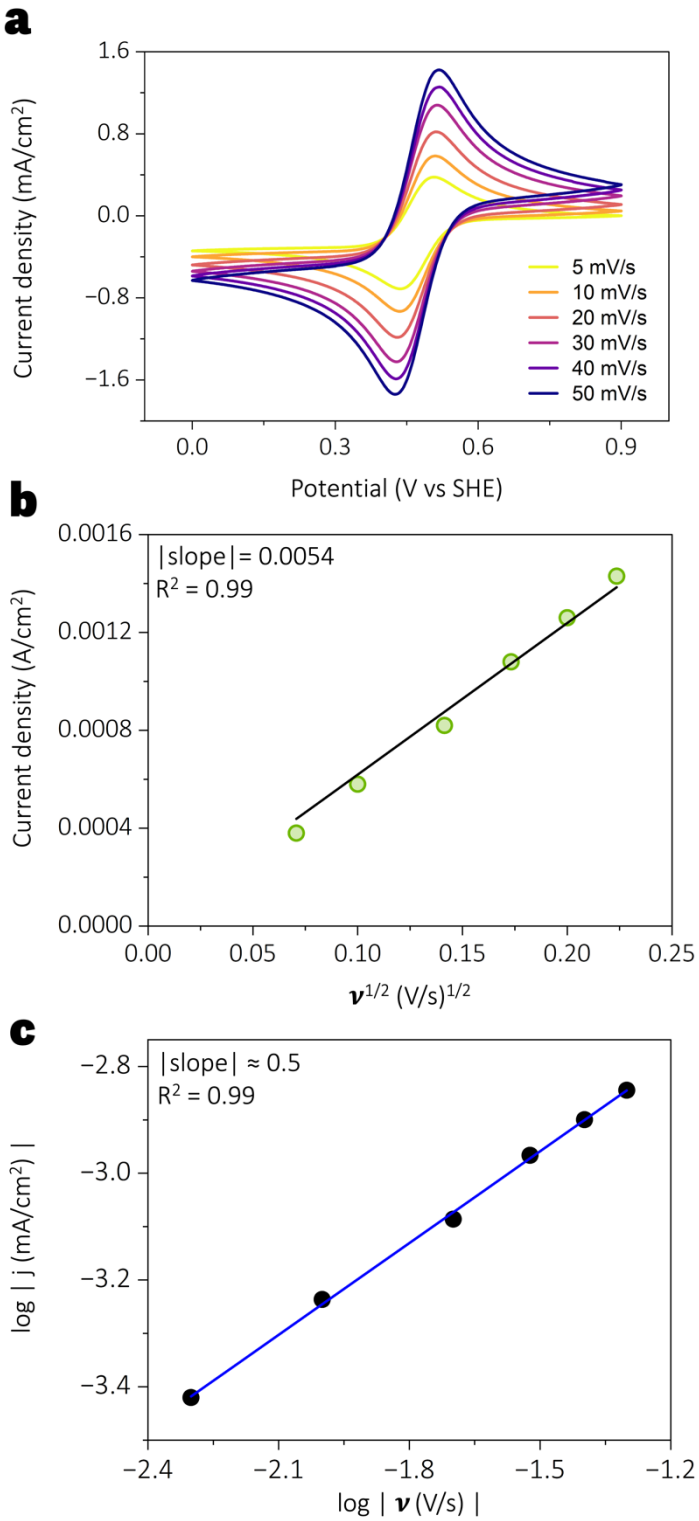

Fig. S2: a) Cyclic voltammetry of 10 mM ferricyanide in 1 M KNO_3 at varying scan rates. b) Linear relationship between peak current density and the square root of scan rate (derived from panel S2a). c) Linear fit of log (current density) versus log (scan rate). Data is extracted from panel S2a.

Calculation S1

The slope of the plot from the scan rate dependence logarithmic plot was used to determine the diffusion coefficient using the Randles-Sevick Equation (Eq. S1):

$I_P = (2.69*10^5)\, n^{3/2}\, A\, D^{1/2}\, \nu^{1/2}\, C,$ Eq. S1

where, I_P= peak current (A), n= number of electrons, A= area of the electrode in cm^2, D= diffusion coefficient (cm^2/s), C= concentration (mol/cm^3) and ν = scan rate (V/s).

n= 1

C = 10 mM = 10^{-5} mol/cm^3

From the slope of Fig. S2b, slope (m) = 0.0054

$0.0054 = 2.69*10^5\, n^{3/2}\, D^{1/2}\, C$

$D = \{0.0054/(2.69*10^5*1*10^{-5})\}^2$

$D = 4.02 * 10^{-6}$ cm^2/s

The diffusion coefficient = $4.02 * 10^{-6}$ cm^2/s

Calculation S2

Number of electron calculation using the Levich equation (Eq. S2),

$I_L = (0.620)\, nFAD^{2/3}\, \nu^{-1/6}\, \omega^{1/2}\, C$ Eq. S2

where I_L= Levich current (A), n= number of electrons, F= Faraday constant (C/mol), A= area of the electrode in cm^2, D= diffusion coefficient (cm^2/s), C= concentration (mol/cm^3), ν = kinematic viscosity (cm^2/s), ω= angular rotation rate of the electrode (rad/s).

Now, the equation in simplified terms,

$I_L = B * \omega^{1/2}$

where, B is the slope of the graph between I_L/A vs $\omega^{1/2}$

$B = (0.620)\, nFD^{2/3}\, \nu^{-1/6}\, C$

F = 96485 C/mol

$D = 4.02 * 10^{-6}\ cm^2/s$

ν = 0.5 cm^2/sec (at 25 °C, 1 atm pressure)

$C = 10^{-5}\ mol/cm^3$

Hence, the slope of the above graph (see Fig. 2e) is 0.131

$B = 0.131\ [(mA/cm^2)/(rad/s)] = 0.000131\ [(A/cm^2)/(rad/s)]$

$0.000131 = (0.620)\, nFAD^{2/3}\, \nu^{-1/6}\, C$

$$n = \frac{0.000131}{0.620 * 96485 * (4.02 * 10^{-6})^{0.667} * (0.5)^{-0.166} * 10^{-5}}$$

$n = 0.78 \approx 1$

Calculation S3

The anodic reaction proceeds mainly to gluconic acid (Eq. S3), which is a 2-electron oxidation per glucose rather than the full 24-electron oxidation to CO_2 (Eq. S4).

Full Oxidation Reaction (24-electron process)

$C_6H_{12}O_6$ (s) + 24 OH^-(aq) → 6 CO_2 (g) + 18 H_2O (l) + 24 e^- Eq. S3

Partial Oxidation Reaction (2-electron process)

$C_6H_{12}O_6$ (s) + 2 OH^-(aq) → $C_6H_{12}O_7$ (s) + H_2O (l) + 2e^- Eq. S4

Charge available per mole of glucose (Faraday constant F=96,485 C mol^{-1})

- 2-electron process: Q_{2e} = 2F =1,92970 C mol^{-1}
- 24-electron process: Q_{24e} = 24F = 23,15,640 C mol^{-1}

Capacity (Ah) per mole (1 A·h = 3600 C)

- Q_{2e} → 53.60 A h mol^{-1}
- Q_{24e} → 643.23 A h mol^{-1}

<u>Charge efficiency comparison</u>

Fraction of charge efficiency by partial oxidation: ~8.3%

In our system, glucose is oxidized mainly to gluconic acid via a 2-electron pathway rather than the full 24-electron oxidation to CO_2. As a result, only ~8.3% of the theoretical charge and energy stored in glucose is electrochemically accessible, even at perfect efficiency. This intrinsically limits the achievable energy density and practical capacity, indicating that the device serves as a proof-of-concept for alternative electron-acceptor strategies rather than maximum energy extraction, while highlighting opportunities for catalyst development to enhance electron transfer.

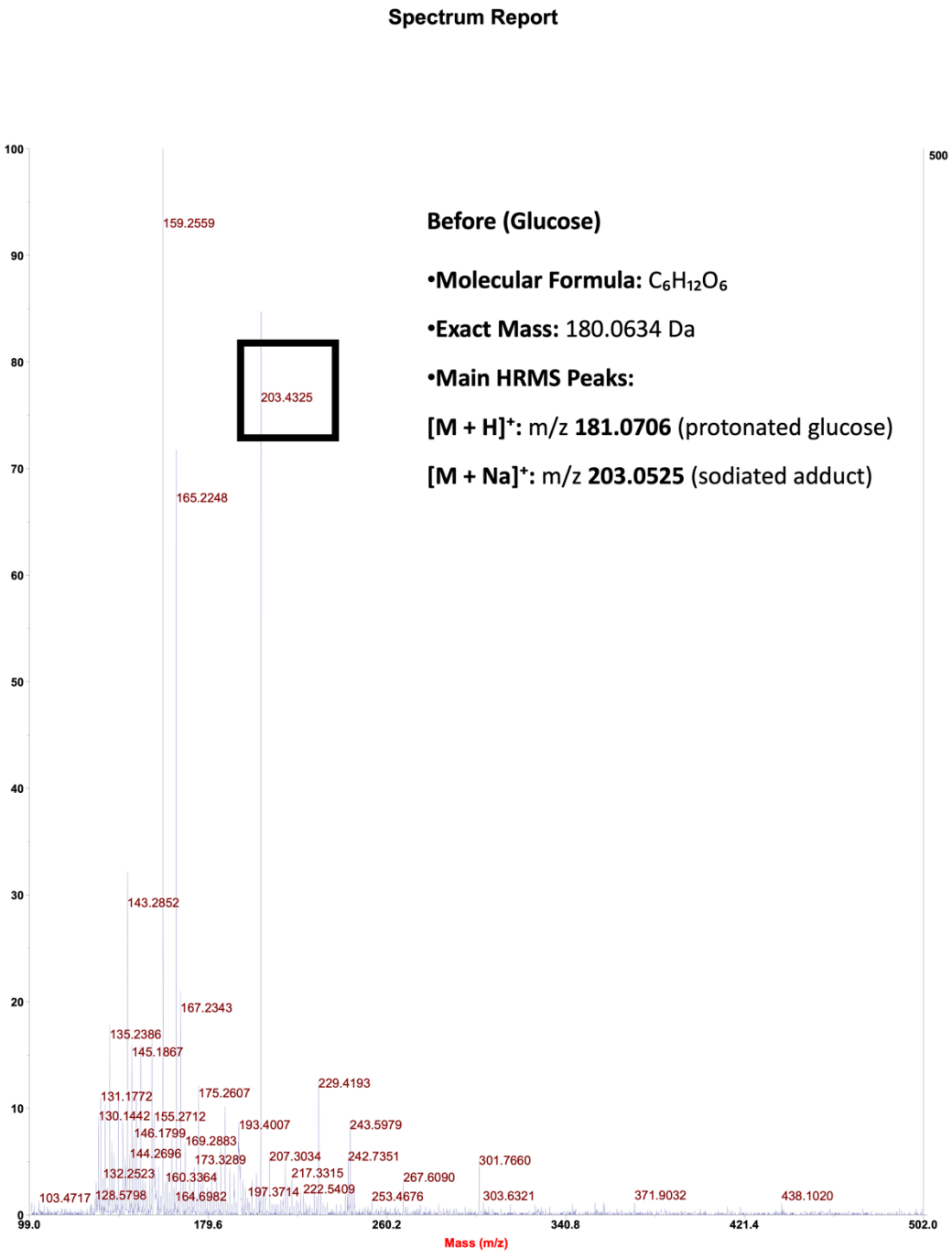

Fig. S3: The high-resolution mass spectrometry (HRMS) spectra of the electrolyte before discharge chemistry. Electrolyte contains glucose dissolved in NaOH.

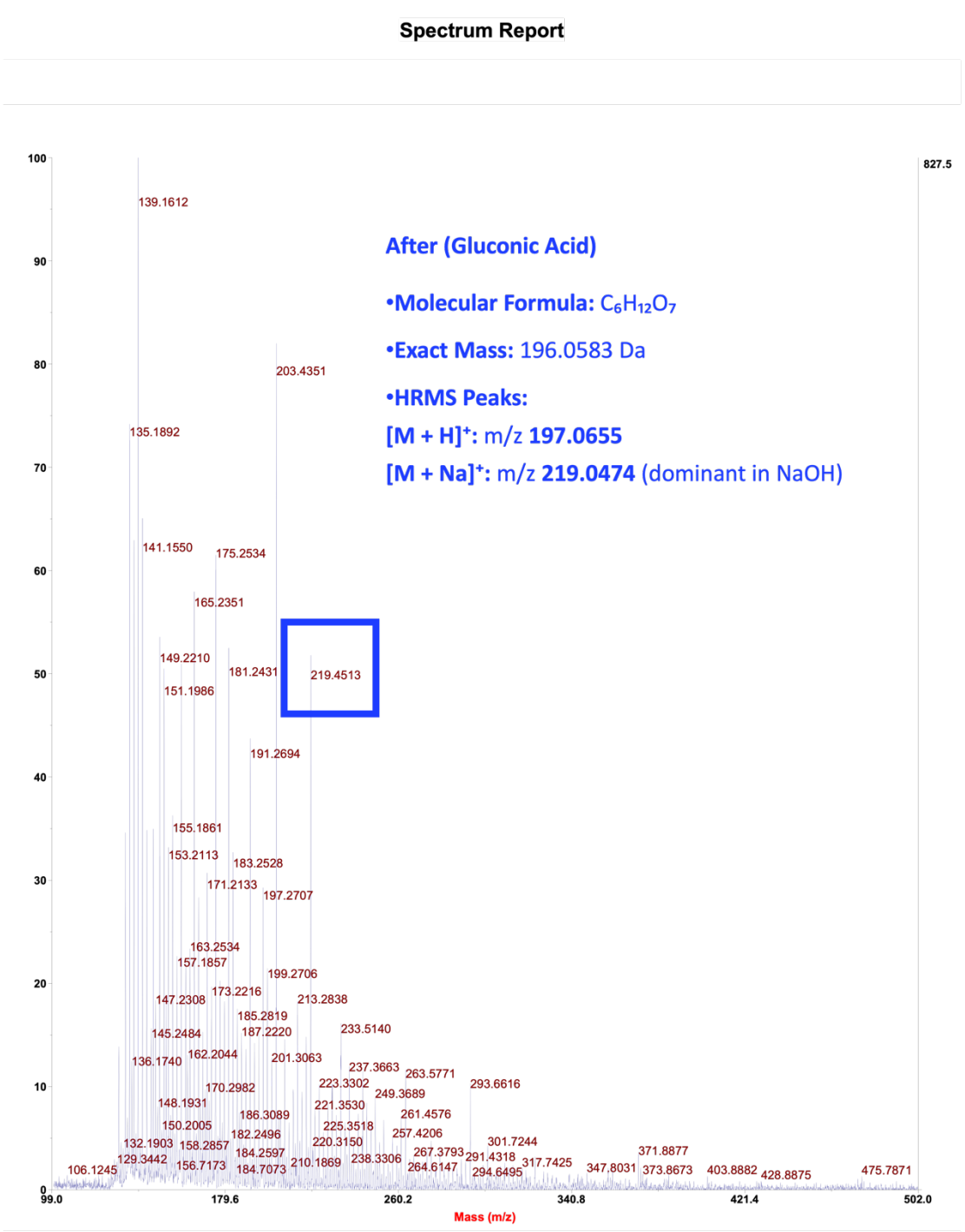

Fig. S4: The high-resolution mass spectrometry (HRMS) spectra of the electrolyte after discharge chemistry. Electrolyte initially contains glucose dissolved in NaOH.

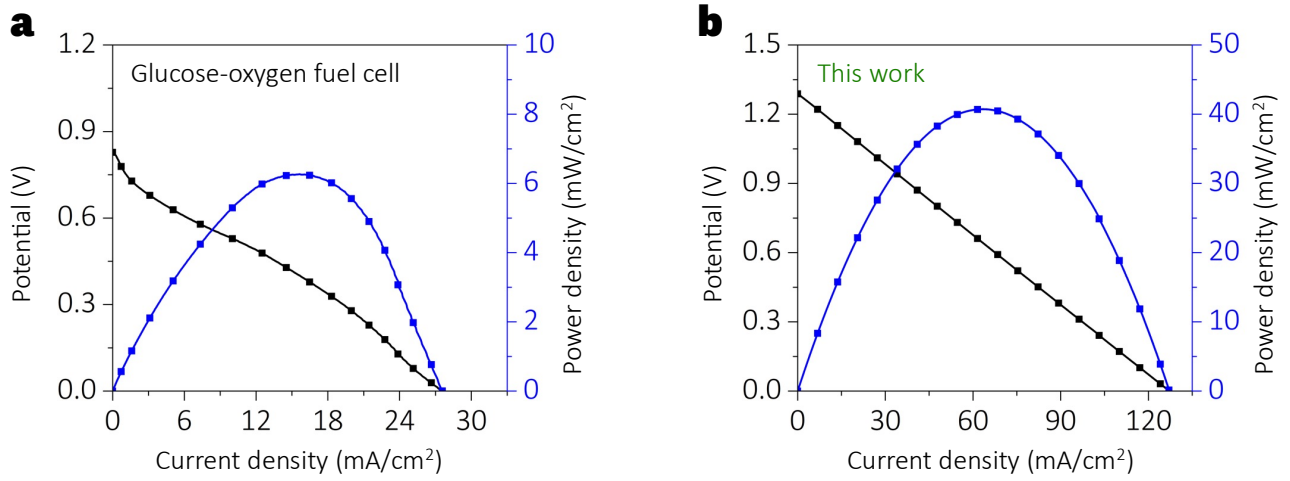

Fig. S5: Polarization curves of (a) the glucose-oxygen fuel cell (cathode: Pt/C, 0.5 mg/cm^2; anode: Pt/C, 0.5 mg/cm^2) Glucose solution was pumped through the anode chamber at 10 mL/min, while oxygen was supplied to the cathode at 100 mL/min. (b) The glucose-ferricyanide system developed in this work (cathode: Pt/C, 0.5 mg/cm^2; anode: carbon). The performance are evaluated under room temperature.

Table S1: Maximum power density comparison with reported state-of-the-art systems employing Pt, Pd, Au-based, and other electrocatalysts.

S.No.	Electrocatalyst	Maximum Power Density (mW/cm^2)	Ref.
Pt-Based Electrocatalyst			
1.	Anode: Pt NFs/CP Cathode: Pt sheet	0.013	S1
2.	Anode: activated C with 10% Pt Cathode: activated C	0.02	S2
3.	Anode: Pt/Au Cathode: Pt	0.022	S3
4.	Anode: Pt/DPtNPs/PtNPs-BC Cathode: Pt/DPtNPs/BC	0.045	S4
5.	Anode: co–Pt Cathode: Ag_2O-MWCNTs	0.062	S5
6.	Anode: Pt-unsupported Cathode: PtRu-unsupported	0.51	S6
7.	Anode: CNT/PDA/GOx/PEI/Nafion Cathode: Pt/C	0.55	S7
8.	Anode: Au/C Cathode: PtAg/C	0.63	S8
9.	Anode: PtRu/C Cathode: activated carbon	1.38	S9
10.	Anode: $PtRuO_2$-unsupported Cathode: Pt-unsupported	1.67	S10
11.	Anode: Pt-Raney Cathode: Pt_{porous}	2	S11
12.	Anode: FTO/TiO2/Pt Cathode: Pt/C	2	S12
13.	Anode: TPA/HRP/GOx/PEI/CNT Cathode: Pt/C-Nafion	2.1	S13
14.	Anode: Pt-Raney Cathode: Pt-Raney	2.2	S11
15.	Anode: PtNi (Raney type)/silicon wafer Cathode: Pt/porous substrate	4.4	S2
16.	Anode: Pt nanoparticles/C Cathode: Co-pthalocyanine/MWCNT	7	S14
17.	Anode: PtAu/C, I/Ca 0.3 Cathode: Pt/C	9.85	S15
Pd-Based Electrocatalyst			
18.	Anode: PdNP/lipid NT	1.9	S16
19.	Anode: $Pd_{30}Au_{70}$/C	2.4	S17
20.	Anode: $Pd_{30}Au_{70}$-NH_3/C	3.0	S18
21.	Anode: Pd_2CeO_2/C	3.4	S19
22.	Anode: PdRh/C	3.5	S20
23.	Anode: Pd_3Sn_2/C/	3.6	S21
Au-Based Electrocatalyst			
24.	Anode: Au	0.014	S22

	Cathode: Pt/Au		
25.	Anode: AuNP/co-Pt Cathode: Ag2O-MWCNT	0.087	S23
26.	Anode: Au (NPG) Cathode: PtNPs@NPG	0.025	S24
27.	Anode: Silver modified Au_{film}/C Cathode: Silver modified Au_{film}/C	0.22	S25
28.	Anode: Au_{film}/glassy carbon Cathode: 3D-Pt_{porous}/$C_{commercial}$	0.30	S26
29.	Anode: Au/PANI/GO_x Cathode: Au/PANI/Lac	0.69	S27
30.	Anode: Pt-Au Cathode: activated charcoal	0.72	S28
31.	Anode: $AuMnO_2$/C Cathode: activated charcoal	1.1	S29
32.	Anode: AuZn/C Cathode: AuZn/C	2.07	S30
33.	Anode: Au nanoporous Cathode: Pt/C commercial	4.4	S31
Other electrocatalyst			
34.	Anode: Co_3O_4-3DrGO/Nif Cathode: N,Fe-PSAC	0.012	S32
35.	Anode: Carbon felt Cathode: MnO2	1.28	S33
36.	Anode: Co3O4/3DGn Cathode: Co3O4/3DGn	2.4	S34
37.	Anode: Carbon felt Cathode: Pt/C	2.5	S35
38.	Anode: FeCo2O4/AC Cathode: Cu2O/Cu/AC	3.5	S36
39.	Anode: Ni_2Co-rGO Cathode: Ni_2Co-rGO	4.04	S37
40.	Anode: rGO-NS–Ni Cathode: rGO-NS	4.8	S38
41.	Anode: PMo12/FeCl3 Cathode: P3Mo18V7	6.5	S39
42.	**Anode: Pt/C** **Cathode: Carbon**	**40.7**	**This work**

References:

S1. X. Xu, X. Dong, D. Li, M. Qi and H. Huang, *ACS Appl. Mater. Interfaces*, 2023, **15**, 17969–17977.
S2. F. Von Stellen, S. Kerzenmacher, A. Lorenz, V. Chokkalingam, N. Miyakawa, R. Zengerle and J. Ducrée, in *Proceedings of the IEEE International Conference on Micro Electro Mechanical Systems (MEMS)*, 2006, vol. 2006, pp. 934–937.
S3. A. Baingane and G. Slaughter, *IEEE Sens. J.*, 2021, **21**, 5751–5757.
S4. M. Yin, J. Chen, J. Sun, J. Fan, D. Li, Z. Zhu and S. Liu, *J. Power Sources*, 2024, **606**, 234542.
S5. S. Banerjee and G. Slaughter, *Sci. Rep.*, 2022, **12**, 12356.
S6. A. Kloke, C. Köhler, R. Zengerle and S. Kerzenmacher, *J. Phys. Chem. C*, 2012, **116**, 19689–19698.
S7. J. Ji, S. Kim, Y. Chung and Y. Kwon, *J. Ind. Eng. Chem.*, 2022, **111**, 263–271.
S8. M. Guerra-Balcázar, F. M. Cuevas-Muñiz, L. Álvarez-Contreras, L. G. Arriaga and J. Ledesma-García, *J. Power Sources*, 2012, **197**, 121–124.
S9. D. Basu and S. Basu, *Electrochim. Acta*, 2010, **55**, 5775–5779.
S10. C. A. Apblett, D. Ingersoll, S. Sarangapani, M. Kelly and P. Atanassov, *J. Electrochem. Soc.*, 2010, **157**, B86.
S11. A. Kloke, B. Biller, S. Kerzenmacher and R. Zengerle, *Eurosensors Proc.*, 2008, 1416–1419.
S12. M. Kaneko, H. Ueno and J. Nemoto, *Catal. Letters*, 2012, **142**, 469–479.
S13. Y. Chung, D. C. Tannia and Y. Kwon, *Chem. Eng. J.*, 2018, **334**, 1085–1092.
S14. R. Haddad, J. Thery, B. Gauthier-Manuel, K. Elouarzaki, M. Holzinger, A. Le Goff, G. Gauthier, J. El Mansouri, A. Martinent and S. Cosnier, *Electrochem. commun.*, 2015, **54**, 10–13.
S15. T. Yuki, N. Katayama, M. Takahashi, K. Tsuchiya, H. Sakai and M. Abe, *ECS Trans.*, 2018, **83**, 145
S16. J. H. Kim and C. S. Yoon, *J. Electroanal. Chem.*, 2021, **900**, 115736.
S17. L. Yan, A. Brouzgou, Y. Meng, M. Xiao, P. Tsiakaras and S. Song, *Appl. Catal. B Environ.*, 2014, **150**–**151**, 268–274.
S18. T. Jiang, L. Yan, Y. Meng, M. Xiao, Z. Wu, P. Tsiakaras and S. Song, *Appl. Catal. B Environ.*, 2015, **162**, 275–281.
S19. S. Song, K. Wang, L. Yan, A. Brouzgou, Y. Zhang, Y. Wang and P. Tsiakaras, *Appl. Catal. B Environ.*, 2015, **176**–**177**, 233–239.
S20. A. Brouzgou, L. L. Yan, S. Q. Song and P. Tsiakaras, *Appl. Catal. B Environ.*, 2014, **147**, 481–489.
S21. A. Brouzgou, S. Song and P. Tsiakaras, *Appl. Catal. B Environ.*, 2014, **158**–**159**, 209–216.
S22. C. Gonzalez-Solino, E. Bernalte, B. Metcalfe, D. Moschou and M. Di Lorenzo, *J. Power Sources*, 2020, **472**, 228530.
S23. S. Banerjee and G. Slaughter, *J. Electroanal. Chem.*, 2022, **904**, 115941.
S24. C. W. Bae, M. V. Chinnamani, E. H. Lee and N.-E. Lee, *Adv. Mater. Interfaces*, 2022, **9**, 2200492.
S25. C. Jin and I. Taniguchi, *Mater. Lett.*, 2007, **61**, 2365–2367.
S26. F. Xie, Z. Huang, C. Chen, Q. Xie, Y. Huang, C. Qin, Y. Liu, Z. Su and S. Yao, *Electrochem. commun.*, 2012, **18**, 108–111.
S27. P. Mishra, G. B. V. S. Lakshmi, S. Mishra, D. K. Avasthi, H. C. Swart, A. P. F. Turner, Y. K. Mishra and A. Tiwari, *Nano Energy*, 2017, **39**, 601–607.
S28. D. Basu and S. Basu, *Electrochim. Acta*, 2011, **56**, 6106–6113.
S29. L. Li, K. Scott and E. H. Yu, *J. Power Sources*, 2013, **221**, 1–5.
S30. H. B. Noh, M. Halappa Naveen, Y. J. Choi, E. S. Choe and Y. B. Shim, *Chem. Commun.*, 2015, **51**, 6659–6662.
S31. X. Yan, X. Ge and S. Cui, *Nanoscale Res. Lett.*, 2011, **6**, 1–6.
S32. T. Purkait and R. S. Dey, *J. Electroanal. Chem.*, 2020, **874**, 114467.
S33. D. M. Scott, T. H. Tsang, L. Chetty, S. Aloi and B. Y. Liaw, *J. Power Sources*, 2011, **196**, 10556–10562.
S34. Y. Chen, K. P. Prasad, X. Wang, H. Pang, R. Yan, A. Than, M. B. Chan-Park and P. Chen, *Phys. Chem. Chem. Phys.*, 2013, **15**, 9170–9176.
S35. D. Scott and B. Y. Liaw, *Energy Environ. Sci.*, 2009, **2**, 965–969.
S36. F. Dong, X. Liu, M. Irfan, L. Yang, S. Li, J. Ding, Y. Li, I. U. Khan and P. Zhang, *Int. J. Hydrogen Energy*, 2019, **44**, 8178–8187.

S37. Y. Li, J. Ding, X. Liu, J. Wang, S. Jiao, N. Kang, J. Li, M. Irfan and P. Zhang, *Biomass Convers. Biorefinery*, 2024, **14**, 525–537.
S38. Y. Dai, J. Ding, J. Li, Y. Li, Y. Zong, P. Zhang, Z. Wang and X. Liu, *Nanomaterials*, 2021, **11,** 202.
S39. Y. Liu and H. Li, *Energy*, 2019, **189**, 116171.